

A hyperspherical-coordinate approach to the spectra and decay widths of hybrid quarkonia

T. Miyamoto^{1,2,*} and S. Yasui^{1,3,†}

¹*Department of Physics, Tokyo Institute of Technology,
Ookayama 2-12-1, Meguro, Tokyo 152-8550, Japan*

²*Graduate School of Engineering Science, Yokohama National University,
Tokiwadai 79-1, Yokohama, Kanagawa 240-8501, Japan*

³*Research and Education Center for Natural Sciences, Keio University,
Hiyoshi 4-1-1, Yokohama, Kanagawa 223-8521, Japan*

(Dated: 14 December 2024)

In this paper, we consider the possibility that $Y(4260)$, $Y(4360)$, $\psi(4415)$ or $X(4660)$ is the ground state or the first excited state of a hybrid charmonium, and examine whether $\Upsilon(10860)$ is the ground state or the first excited state of a hybrid bottomonium. Under a constituent quark model, we carry out numerical calculations to obtain the spectra of both electric-gluon and magnetic-gluon hybrid quarkonia. We see that the ground state of a magnetic-gluon hybrid charmonium and the first excited state of an electric-gluon hybrid are comparable in energy to $\psi(4415)$, and that the first excited states of an electric-gluon hybrid bottomonium and the ground state of an magnetic-gluon hybrid appear a few hundred MeV above the mass of $\Upsilon(10860)$. Also, we evaluate the widths of the decays of a hybrid charmonium into $D^{(*)}\bar{D}^{(*)}$ and those of a hybrid bottomonium into $B^{(*)}\bar{B}^{(*)}$. We show that if the exotic meson candidates are hybrid charmonia, then they are magnetic-gluon ones, and argue that it seems unlikely that $\Upsilon(10860)$ is the ground state of an electric-gluon hybrid bottomonium.

I. INTRODUCTION

Over the past decades, research on exotic hadrons has been one of the most important areas of research in terms of Quantum Chromodynamics (QCD), given that the quantum field theory of the strong interaction does not deny the existence of colour-singlet particles of this sort. Year 2003 marked the beginning of a new chapter in the history of QCD, because $X(3872)$, the first exotic meson candidate, was observed at Belle [1]. The discovery of $X(3872)$ accelerated the trend of research on exotic hadrons: since then, various exotic meson candidates have been found, and the possibility of existence of further exotic hadrons has been raised. This has provided a huge motivation to further search for exotic hadrons [2], and led to a better understanding of how the experimentally-verified exotic hadron candidates are described.

Among those exotic hadron candidates, $Y(4260)$, which was first observed in 2005, is singled out for special treatment. Using initial state radiation (ISR), BaBar Collaboration revealed the existence of the particle [3], and it was subsequently confirmed by the CLEO-c [4] and Belle experiments [5]. Also, it was confirmed that the particle has $J^{PC} = 1^{--}$, as the measured dipion mass distribution agreed with the distribution that was calculated in an S-wave phase space model [6]. There are several reasons why $Y(4260)$ has been regarded as

a highly exotic meson: the decay width of the process $Y(4260) \rightarrow J/\psi \pi^+ \pi^-$ is significantly large compared to that of other vector charmonia such as $\psi(4040)$; $Y(4260)$'s decay into $D\bar{D}$ has not been observed; the decay width of the process $Y(4260) \rightarrow \psi \pi^+ \pi^-$ was larger than 5.0 MeV, much larger than that of other 1^{--} charmonium mesons such as $\psi(3770)$ (80-90 keV) and $\psi(4040)$ ($\leq 100 \pm 30$ keV) [7]; also $Y(4260)$ decays into an exotic meson $Z(3900)^\pm$ [8].

From a theoretical point of view, there are the following several arguments to explain the anomalous behaviour of $Y(4260)$. Firstly, it could be argued that the particle is a $c\bar{c}s\bar{s}$ tetraquark, although the decay channel $Y(4260) \rightarrow D_s \bar{D}_s$ has not been observed yet. Secondly, the possibility that $Y(4260)$ is a $\bar{D}D_1(2420)$ molecule has been raised [9], while there is an argument that the binding energy extracted from the experimental data is stronger than the energy scale that is related to the Yukawa meson exchange interaction. Also, the particle could be interpreted as a hadrocharmonium, that is, a charmonium surrounded by the cloud of light hadrons [10].

Another interpretation has been put on the experimental results: the particle is a hybrid charmonium which consists of $c\bar{c}$ and a constituent gluon [11]. As a hybrid meson must conform to its selection rule [12], the ground state of a hybrid charmonium could have either an electric or a magnetic gluon. The decay pattern of $Y(4260)$ suggests that the constituent gluon should be magnetic.

In relation to a charmonium hybrid, let us note that several hybrid mesons have been considered; for the details of light hybrids see the review paper which was written by Meyer and Swanson [13].

* miyamoto-tomokazu-gv@ynu.ac.jp,
tomokazu.miyamoto10@physics.org

† yasuis@keio.jp

Under the assumption that a charmonium hybrid exists, it is possible that there could exist a bottomonium-equivalent of the hybrid meson; several different theoretical studies have explored the possibility of a hybrid bottomonium. For instance, a lattice QCD calculation which employed a non-relativistic approach showed that the gluonic excitation could exist 1.542 GeV above the "ground" state (≈ 9.45 GeV) [13, 14]. Another lattice calculation, together with the leading Born Oppenheimer (LBO) approximation, suggested that the lowest hybrid state could exist 1.49 GeV above the 1S state [15]. Also, the QCD sum rule analyses predicted that there exist several bottomonium hybrids: $J^{PC} = 0^{-+}$ at around 10.6 ± 0.19 GeV [16]; 1^{--} in the mass range of 10.24 to 11.15 GeV [17]; and 1^{++} at around 11.32 ± 0.32 GeV [18]. Furthermore, it has been reported that the spin-dependent structures of hybrid quarkonia were unveiled within the Born-Oppenheimer Effective Field Theory (BOEFT) framework [19].

Experimentalists have not yet obtained conclusive evidence that the gluonic degrees of freedom could appear in a bottomonium. However, we can spotlight a few particles which sit above the $B\bar{B}$ threshold: $Y_b(10890)$ is said to be a candidate for a $b\bar{b}g$ [20]; and the anomalously large partial width concerning the decays of $\Upsilon(10860)$ (or $\Upsilon(5S)$) into $\Upsilon(nS)\pi^-\pi^+$ should be looked at more carefully.

Hybrid quarkonia have opened up an opportunity to not only study the gluonic degrees of freedom but also assess how a quark and its antiquark interacts in a $q\bar{q}g$. While the $q\bar{q}$ of a usual quarkonium are bound together by the static quark potential, which is not directly measurable in an experiment, a hybrid quarkonium emerge from the excitations of dynamical gluon. The excitations were studied within the lattice framework [21]; at the same time, it is possible to interpret the gluonic excitations as the string vibration modes under the flux tube regime [22]. The Lüscher term approach can also be used to assess the gluonic excitations [23], which is helpful in placing the constraints on the effective interactions relating to the mixing between hybrids and heavy quarkonium states [24].

In the present paper, we consider the possibility that $Y(4260)$ or one of the other related exotic meson candidates such as $Y(4360)$ is the ground state or the first excited state of a hybrid charmonium, and examine whether $\Upsilon(10860)$ is the ground state or the first excited state of a hybrid bottomonium. Under a semi-relativistic framework, we calculate the energy spectra of a charmonium and bottomonium hybrids, and obtain the quark-antiquark effective potentials. Recognising QCD's non-perturbative nature, we adopt a constituent quark model in which the whole system consists of a quark, its antiquark and a constituent gluon. Also, we consider the decays of a charmonium hybrid and bottomonium hybrid into $D^{(*)}\bar{D}^{(*)}$ and $B^{(*)}\bar{B}^{(*)}$, respectively, evaluating these decay widths.

Section 2 consists of several subsections: the auxil-

ary field approach, hyperspherical formalism, the quark-antiquark effective potentials and the decays of a hybrid charmonium into $D^{(*)}\bar{D}^{(*)}$ and those of a hybrid bottomonium into $B^{(*)}\bar{B}^{(*)}$. In Section 3, we present our numerical results. The summary is given in the final section.

II. FORMALISM

A. The model for a hybrid meson

In this subsection, we begin by introducing the Hamiltonian of the whole system $q\bar{q}g$, where q and \bar{q} stand for a heavy quark and its antiquark, respectively. According to earlier studies conducted by Kalashnikova and (subsequently Mathieu), the total Hamiltonian of a hybrid meson is given as the sum of the free Hamiltonian and the potential [25, 26]: $H = H_f + V$. The free Hamiltonian and the potential term are expressed as follows:

$$H_f = \sqrt{\mathbf{p}_q^2 + m_q^2} + \sqrt{\mathbf{p}_{\bar{q}}^2 + m_{\bar{q}}^2} + \sqrt{\mathbf{p}_g^2}, \quad (1)$$

$$V = \sigma r_{qg} + \sigma r_{\bar{q}g} + V_C, \quad (2)$$

where m_q and \mathbf{p}_q are the mass and the momentum of a quark, respectively. Likewise, subscripts \bar{q} and g denote an antiquark and a constituent gluon. In this model, the mass m_g of the constituent gluon is strictly zero.

When it comes to the potentials in the Hamiltonian, σr_{qg} and $\sigma r_{\bar{q}g}$ are the linear potentials for the quark confinement, and V_C is the colour-Coulomb potential for this system. In relations to the potentials, the Casimir scaling is considered: using the SU(3) generators $\{\lambda_i^a\}_{a=1,\dots,8}$, we have the following relations for a hybrid meson:

$$\frac{1}{4}\langle\lambda_q \cdot \lambda_g\rangle = \frac{1}{4}\langle\lambda_{\bar{q}} \cdot \lambda_g\rangle = -\frac{3}{2}, \quad \frac{1}{4}\langle\lambda_q \cdot \lambda_{\bar{q}}\rangle = \frac{1}{6}. \quad (3)$$

Accordingly, we have the expressions for V_C :

$$V_C = -\frac{3\alpha_s}{2r_{qg}} - \frac{3\alpha_s}{2r_{\bar{q}g}} + \frac{\alpha_s}{6r_{q\bar{q}}}. \quad (4)$$

The Salpeter-type Hamiltonian in (1) contains square roots, and so does the corresponding action. In general, this sort of square-root has two difficulties: quantisation and dealing with a massless particle [27]. Specifically, in the present paper, we need to consider the constituent gluon which is massless. For these reasons, we adopt the auxiliary field method [28] which involves an auxiliary field μ (or an einbein field) to reparametrise this kind of Hamiltonian:

$$\sqrt{\mathbf{p}^2 + m^2} \Rightarrow \frac{\mathbf{p}^2 + m^2}{2\mu} + \frac{\mu}{2}. \quad (5)$$

The relation (5) suggests that the physical meaning of the auxiliary field μ is that it is the effective mass of a particle [29].

Using the auxiliary field method, and choosing the centre-of-mass of the three-body system as the coordinate origin, we reparametrise the free Hamiltonian (1) by the auxiliary fields $\mu_q, \mu_{\bar{q}}$ and μ_g of the quark, antiquark and constituent gluon, respectively:

$$H_f = \frac{\mu_q + \mu_{\bar{q}} + \mu_g}{2} + \frac{\mathbf{p}_q^2 + m_q^2}{2\mu_q} + \frac{\mathbf{p}_{\bar{q}}^2 + m_{\bar{q}}^2}{2\mu_{\bar{q}}} + \frac{\mathbf{p}_g^2}{2\mu_g}, \quad (6)$$

$$= \frac{\mu_q + \mu_{\bar{q}} + \mu_g}{2} + \frac{m_q^2}{2\mu_q} + \frac{m_{\bar{q}}^2}{2\mu_{\bar{q}}} + \frac{\mathbf{k}_x^2}{2\mu_x} + \frac{\mathbf{k}_y^2}{2\mu_y}, \quad (7)$$

where μ_x and μ_y are defined by

$$\mu_x = \frac{\mu_{\bar{q}}}{2} = \mu_{q\bar{q}}, \quad \mu_y = \frac{2\mu_{\bar{q}}\mu_g}{2\mu_{\bar{q}} + \mu_g}. \quad (8)$$

Also, \mathbf{k}_x and \mathbf{k}_y are the momenta which are defined in the three-body Jacobi coordinates; the details of the coordinates are written in Appendix A.

Strictly speaking, auxiliary fields are dynamical variables, and we need the fields before quantisation. But it is difficult to do that; therefore we here treat the fields ($\mu_q, \mu_{\bar{q}}$ and μ_g) as an approximate variational parameters [28] in order to determine the ground state of the whole system. We also note that an auxiliary field method leads to, at worst, seven per cent disagreement between a numerical value and its true value in a numerical calculation [29].

B. Hyperspherical coordinates

Now we point out that we can take advantage of the auxiliary fields for the linear potentials of (2) in order to treat the reparametrised Hamiltonian (7) as a harmonic oscillator system [32]. However, this sort of analytical treatment does not work properly under the presence of the colour-Coulomb force V_C , as the whole interactions cannot be expressed as harmonic oscillators. Admittedly, instead of doing that kind of analytic calculations, we need to carry out numerical calculations in the present case, adopting a hyperspherical-coordinate approach.

This framework provides a useful tool to study few-body systems such as hadrons and atomic nuclei (see [30], [31] for more details); in fact it was adopted in earlier research on a hybrid charmonium [25]. In this section, we therefore explain the hyperspherical formalism to solve the boundary value problems involving the Hamiltonian.

For convenience, we label each of the constituents of the three-body system by Particle 1, 2 and 3, where Particle 1 and 2 correspond to a quark and an antiquark, respectively. Particle 3 refers to a constituent gluon in this case. Here we use the Jacobi coordinates for the three-body system; the details of the coordinates are shown in Appendix A.

Suppose, in the Jacobi coordinates, X is the distance between Particle 1 and 2, and Y is the distance between Particle 3 and the centre-of-mass of Particle 1 and 2. Then, we introduce the hyperspherical coordinates (ρ, α) as follows:

$$x = \rho \cos \alpha = \sqrt{\mu_{12}}X, \quad y = \rho \sin \alpha = \sqrt{\mu_{12,3}}Y, \quad (9)$$

where ρ is hyperradius and α ($\in [0, \frac{\pi}{2}]$) is hyperangle. For later convenience, we use a shorthand notation Ω_5 to express the set of five angular variables: $\Omega_5 = \{\alpha, \theta_x, \phi_x, \theta_y, \phi_y\}$, where θ_x and ϕ_x are the polar and azimuthal angles of the \mathbf{X} vector, respectively. Similarly, we have for the \mathbf{Y} vector.

The hyperspherical harmonics(HH) is equipped with its relating quantum numbers: K is called the hyperangular momentum; L_x is the orbital angular momentum between Particle 1 and 2; L_y is that between Particle 3 and the centre-of-mass of Particle 1 and 2. Also, an integer n is defined by:

$$K = L_x + L_y + 2n. \quad (10)$$

With these quantum numbers we introduce the HH for the three-body system:

$$\mathcal{Y}_{KLM_L}^{L_x L_y}(\Omega_5) \stackrel{\text{def}}{=} \mathcal{N}(K, L_x, L_y) A_n^{L_x L_y}(\alpha) \times [Y_{L_x}(\Omega_x) \otimes Y_{L_y}(\Omega_y)]_{L_{tot} M_{L_{tot}}}, \quad (11)$$

where we define the hyperangular part $A_n^{L_x L_y}(\alpha)$, by using the Jacobi polynomials $\{P_n^{\alpha, \beta}\}$, as follows:

$$A_n^{L_x L_y}(\alpha) = (\cos \alpha)^{L_x} (\sin \alpha)^{L_y} P_n^{L_y+1/2, L_x+1/2}(\cos 2\alpha). \quad (12)$$

Here $\mathcal{N}(K, L_x, L_y)$ which appears in (11) is a normalisation constant given by:

$$\mathcal{N}(K, L_x, L_y) = \sqrt{2(K+2)} \sqrt{\frac{\Gamma(n+1)\Gamma(L_x+L_y+n+2)}{\Gamma(L_x+n+\frac{3}{2})\Gamma(L_y+n+\frac{3}{2})}}. \quad (13)$$

In the present method, the total wave function is expanded with regard to the HH:

$$\begin{aligned} \Psi_{JM_J}(\mathbf{x}, \mathbf{y}) &= \frac{1}{\rho^{5/2}} \sum_{K\gamma} \chi_{K\gamma}(\rho) [\mathcal{Y}_{K L_{tot}}^{L_x L_y}(\Omega_5) \otimes |S_{tot}\rangle]_{JM_J} \\ &= \frac{1}{\rho^{5/2}} \sum_{K\gamma} \chi_{K\gamma}(\rho) \Upsilon_{K\gamma JM_J}, \end{aligned} \quad (14)$$

where $\{\chi_{K\gamma}(\rho)\}_{K,\gamma}$ are the hyperradial functions of the whole wave function, and $|S_{tot} M_{S_{tot}}\rangle$ is the spin part, and γ is a set of quantum numbers: $\gamma = \{L_{tot}, S_{tot}, L_x, L_y\}$. We also note that $\Upsilon_{K\gamma JM_J}(\Omega_5)$ is given by $\Upsilon_{K\gamma JM_J}(\Omega_5) = [\mathcal{Y}_{K L_{tot}}^{L_x L_y} \otimes |S_{tot}\rangle]_{JM_J}$.

In actual calculations, we need to numerically obtain the hyperradial functions. To do this, we substitute (14) into the Schrödinger equation, which yields the following a set of inhomogeneous differential equations (hyperradial equations):

$$\frac{-1}{2} \left(\frac{\partial^2}{\partial \rho^2} - \frac{(K+3/2)(K+5/2)}{\rho^2} \right) \chi_{K\gamma} + \sum_{K\gamma} V_{K\gamma K',\gamma'} \chi_{K'\gamma'} = E \chi_{K\gamma}, \quad (15)$$

where the matrix element of a potential is defined by

$$V_{K\gamma, K'\gamma'} \stackrel{\text{def}}{=} \langle \Upsilon_{K\gamma}(\Omega_5) | V_{12} + V_{23} + V_{31} | \Upsilon_{K'\gamma'}(\Omega_5) \rangle. \quad (16)$$

Thus we see that the three-body problem is reduced to dealing with a one-dimensional problem, but we are still confronted with the inhomogeneous equations. Here we address the problem by expanding each of the hyper-radial functions with regard to a generalised Laguerre-based basis function in one-dimensional space:

$$\chi_{K\gamma} = \sum_{j=0}^{B-1} a_j^{(m)} u_{\alpha,j}(\rho), \quad (17)$$

where B is the number of the basis functions. The generalised Laguerre-based basis functions $\{u_{\alpha,j}\}$ are defined by

$$u_{\alpha,j}(z) = \sqrt{\frac{\Gamma(j+1)}{\Gamma(\alpha+j+1)}} e^{-\frac{z}{2}} z^{\frac{\alpha}{2}} L_j^{(\alpha)}(z). \quad (18)$$

By virtue of this, our problem is reduced to solving the boundary value problems which involve $a_j^{(m)}$. We note that here m is a set of quantum numbers: $m = \{K, \gamma\}$. In the present case, we set $\alpha = 5$.

The whole wave function Ψ is normalised as:

$$\int |\Psi_{JM_J}|^2 d\mathbf{x} d\mathbf{y} = \sum_{K\gamma} \int_0^\infty |\chi_{K\gamma}|^2 d\rho = 1. \quad (19)$$

C. Effective potential of a colour-octet quark-antiquark pair

As mentioned earlier, standard quarkonium states emerge from the static quark potential, while the excitations of dynamic gluons are responsible for hybrid meson states. From a constituent quark model perspective, the gluonic excitations are described by the effective potential with which the constituent gluon of a $q\bar{q}g$ involves, keeping the quark-antiquark subsystem colour-octet. In other words, the information about the gluonic degrees of freedom can be accessed through studying the quark-antiquark effective potential.

In this subsection, therefore we calculate the quark-antiquark effective potentials in a $q\bar{q}g$. The effective potential is derived from integrating over the coordinates \mathbf{Y} relating to the constituent gluon of a hybrid meson:

$$\hat{V}(\mathbf{X}) = \langle g | V(\mathbf{X}, \mathbf{Y}) | g \rangle, \quad (20)$$

where coordinates \mathbf{X} represent the $q\bar{q}$ relative position.

Our approach to derive the effective potential is to take advantage of the Lagrange mesh method (LMM). Details of the LMM is given in Appendix C. Suppose that the eigen-energy E and the whole wave function of a physical system are given. Then, the procedure for calculating the potentials consists of two parts: we extract a two-body radial wave function $R(X)$ from the whole wave function; then we obtain the effective potential relating the subsystem by solving the inverse problem.

The two-body radial wave function $R(X)$ of a colour-octet subsystem $q\bar{q}$ by solving the following equation:

$$R(X) = \int |\Psi(\mathbf{X}, \mathbf{Y})|^2 d\mathbf{Y} d\Omega_X, \quad (21)$$

where Ω_X is a shorthand notation for the angular variables of the \mathbf{X} vector. Then, after normalising $R(X)$, we obtain a dimensionless wave function by $\phi_X(X) = XR(X)$. By using the dimensionless two-body radial wave function, we solve the inverse problems in terms of the Hamiltonian of the subsystem in order to obtain the effective potential:

$$\hat{V}(x_i) = E - \sum_{j=1}^N T_{ij} \frac{\sqrt{\lambda_j} \phi(x_j)}{\sqrt{\lambda_i} \phi(x_i)}, \quad (22)$$

where $\{T_{ij}\}_{i,j}$ are the matrix elements of the Hamiltonian. $\{x_i\}_i$ and $\{\lambda_i\}_i$ are defined in Appendix C.

D. Decays of hybrid mesons

Now we consider the decays of a hybrid charmonium into $D^{(*)}\bar{D}^{(*)}$. Under the selection rules, a magnetic-gluon $c\bar{c}g$ does not get involved in these processes [11], and therefore we consider only electric-gluon hybrids.

In the present case, we consider the lowest-order decay, as is shown in Figure 1. Its formalism was already presented in earlier research [12, 33], where the wave functions of the initial and final particles were described by Gaussian-type functions. The final states are treated in a non-relativistic way, given the fact that the mass of a D meson is at lightest about 1.86 GeV. Also, we note that this method could be more suitable for calculating the widths of the decays of a $b\bar{b}g$ into $B^{(*)}\bar{B}^{(*)}$, because the final mesons are much heavier so that the non-relativistic approximation is more reasonable.

The initial and final wave functions of a $c\bar{c}g$ influence the decay amplitude $f_{A \rightarrow BC}$ (whose details are shown in

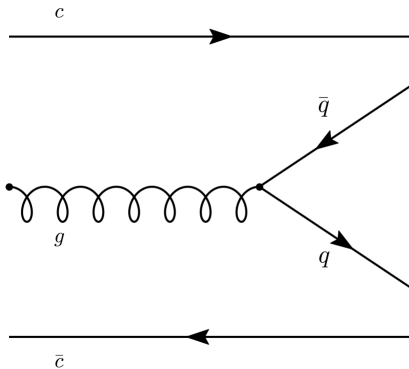


Figure 1. $D\bar{D}$ decay channel of a $c\bar{c}g$.

[33]). In the present work, obtaining the wave functions of an initial state, we use the momentum representation to calculate the decay widths (for the details of the representation, see Appendix D.) Also, we take account of the effects of correlation between the charm-anticharm pair and the constituent gluon of a $c\bar{c}g$.

Suppose a $c\bar{c}g$ is particle A, and D and \bar{D} mesons are particle B and C, respectively. Here we denote their masses by m_A , m_B and m_C . Then, the decay width $\Gamma_{A\rightarrow BC}$ regarding the process is expressed as

$$\Gamma_{A\rightarrow BC} = 4\alpha_s |f_{A\rightarrow BC}|^2 \frac{P_B E_B E_C}{m_A}, \quad (23)$$

where E_B and E_C are the energies of particle B and C, respectively: $E_B = \sqrt{P_B^2 + m_B^2}$ and $E_C = \sqrt{P_B^2 + m_C^2}$. We also note that here P_B is given by

$$P_B = \frac{1}{2m_A} \cdot \sqrt{\{m_A^2 - (m_B + m_C)^2\}\{m_A^2 - (m_B - m_C)^2\}}. \quad (24)$$

III. RESULTS

In this section, we present the results of our numerical calculations with respect to hybrid quarkonia. We begin by distinguishing the magnetic gluon case from the electric, using the parity P and C-parity C of a hybrid meson: they are given by $P = (-1)^{L_{q\bar{q}}+L_g}$, $C = (-1)^{L_{q\bar{q}}+S_{q\bar{q}}+1}$; also we have the relation of $L_g = J_g$ for a magnetic gluon and $L_g = J_g \pm 1$ for an electric gluon [12]. Taking these things into account, we show the low-lying states which are allowed to exist for a hybrid meson $q\bar{q}g$ in Table I.

For the magnetic-gluon $q\bar{q}g$, we restrict ourselves to the case where $S_{q\bar{q}} = 0$ and $J^{PC} = 1^{--}$, mentioning that $S_{q\bar{q}} = 1$ leads to $J^{PC} = (0, 1, 2)^{-+}$ [26]. The specific values of the other quantum numbers such as $L_{q\bar{q}}$ are

shown in Table I. Strictly speaking, we need to consider higher values for the quantum numbers, but here we stick to the approximations. Similarly, we consider only $S_{q\bar{q}} = 1$ for the electric gluon, pointing out that, in this case, $J^{PC} = 1^{--}$ does not involve the spin singlet state of the quark-antiquark pair.

gluon	$L_{q\bar{q}}$	L_g	L_{tot}	$S_{q\bar{q}}$	S_g	S_{tot}	$J_{q\bar{q}}$	J_g	J^{PC}
E	1	0	1	1	1	0, 1, 2	$(0, 1, 2)^{++}$	1^-	1^{--}
M	0	1	1	0	1	1	0^{-+}	1^+	1^{--}

Table I. Possible low-lying states for a hybrid meson. In the column of gluon, E and M mean electric gluon and magnetic, respectively.

A. Charmonium hybrid

We now focus on the spectrum of a charmonium hybrid $c\bar{c}g$. As to the parameters relating to the potentials in the Hamiltonian, we set the string tension σ and colour-Coulomb parameter α_s 0.16 GeV² and 0.55, respectively. Here we used 1.48 GeV for the mass m_c of the charm quark [25]. This parameter setting reproduced the energy spectrum of the charmonium to the extent that the difference between our calculation and the experimental data was less than 1 per cent.

Then, taking advantage of the auxiliary field method, we obtain the effective masses ($\mu_c = \mu_{\bar{c}}$ and μ_g) of a charm, anticharm and constituent gluon. The results are shown in Figure 2, where the calculated ground state masses are plotted as functions of μ_c and μ_g . As to the

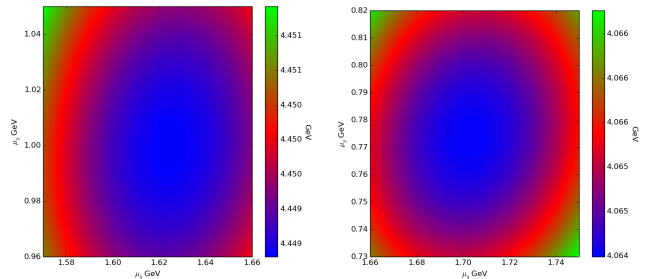


Figure 2. The calculated ground state masses (GeV) of a $c\bar{c}g$ as functions of the auxiliary fields μ_c and μ_g . The left graph is for the magnetic gluon case, and the right for the electric.

values of $\gamma = \{L_{tot}, S_{tot}, L_{c\bar{c}}, L_g\}$, we used Table I to determine it according to the types of the constituent gluon (i.e. electric or magnetic). Here we retained the maximum of the hyperangular momentum K up to 9, which allowed us to see a reasonable convergence (See Figure 3).

Then, the resulting basic parameters regarding the spectrum of a $c\bar{c}g$ are shown in Table II.

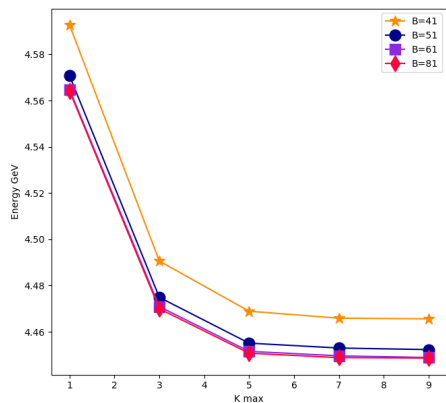


Figure 3. The ground state energies of $c\bar{c}g$ as a function of the maximum of K . B is the number of the generalised Laguerre-based basis functions.

In earlier research a single Gaussian was used as their basis function [25], while we used multi-component generalised Laguerre-based functions to express the hyperradial functions. For this reason, the ground state energy that (≈ 4.448 GeV) we obtained was lower than that (4.573 GeV) they did [26]. In relation to this, we mention that if we use a single-component basis function, then the ground state energy is consistent with their result.

When it comes to the Gaussian correlated approach, the ground state energy for the magnetic case was 4.445 GeV [26]. Figure 3 shows that our results are consistent with it.

σ GeV ²	α_s	m_c GeV	J^{PC}	gluon	μ_c GeV	μ_g GeV
0.16	0.55	1.48	1^{--}	M	1.62	1.00
0.16	0.55	1.48	1^{--}	E	1.70	0.77

Table II. The parameters relating to the spectra of a $c\bar{c}g$. E and M in the gluon column of the table means the electric gluon case and magnetic, respectively.

Next we present the mass spectra of a $c\bar{c}g$ in the right part of Figure 4. From the graph, it is apparent that for the electric gluon case we have lower masses as a whole, compared to the electric. We can see that the ground state of an electric-gluon $c\bar{c}g$ appears about 200 MeV below the mass of $Y(4260)$, while the first excited state of an electric-gluon hybrid and the ground state of a magnetic-gluon hybrid are comparable in energy to $\psi(4415)$.

Then we consider the relation between the mass and RMS radius in terms of a charmonium hybrid for both the magnetic gluon and electric. In the left part of Figure 4, the RMS radii $\sqrt{\langle X^2 \rangle}$ and $\sqrt{\langle Y^2 \rangle}$ for a $c\bar{c}g$ are plotted against the masses of the hybrid, where X is the distance between c and \bar{c} , and Y is the distance between the centre-of-mass of $c\bar{c}$ and a constituent gluon. We can see on this graph that $\sqrt{\langle X^2 \rangle}$ for the electric is as a

whole larger than that for the magnetic case; the same thing holds true for $\sqrt{\langle Y^2 \rangle}$. This result is consistent with our findings about the spectra.

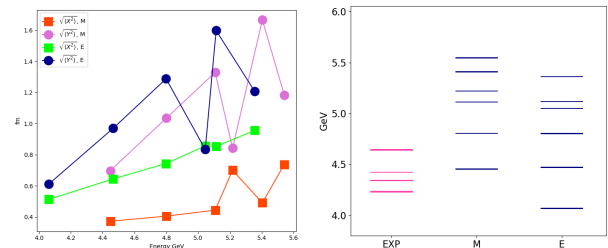


Figure 4. In the left graph, the rms radii $\sqrt{\langle X^2 \rangle}$ and $\sqrt{\langle Y^2 \rangle}$ regarding a $c\bar{c}g$ are plotted against its eigen-energies. In the right figure, the relevant experimental data ($Y(4260)$, $Y(4360)$, $\psi(4415)$, and $X(4660)$) and the calculated energy spectra are shown [34], where E stands for the electric case and M for the magnetic.

Also, the probability densities of a $c\bar{c}g$ for its ground states are shown in Figure 5, where density distributions are scaled so that their peaks and bottoms are set unity and zero, respectively. On these graphs, we see the broad configuration in the Y direction for the magnetic case, while the density distribution has a rather long tail in the X direction for the electric. These spatial configurations are consistent with the fact that a constituent gluon sits in the P state and the orbital angular momentum between c and \bar{c} is zero for the magnetic case, and that a constituent gluon sits in the S state and the orbital angular momentum between c and \bar{c} is one for the electric.

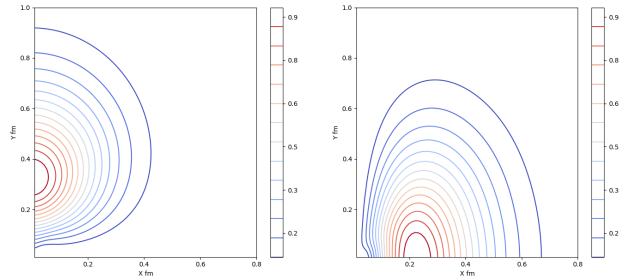


Figure 5. The scaled probability densities of the ground states of a $c\bar{c}g$ for the magnetic case (left) and the electric (right). The density distributions are scaled so that their peaks are unity and their bottoms are zero.

B. Bottomonium hybrid

We then move on to consider a heavier hybrid meson $b\bar{b}g$. Before calculating the energy spectra of a hybrid bottomonium, we need to obtain relevant parameters: the mass m_b of a bottom quark and the colour-Coulomb

parameter α_s . These parameters are fitted to the experimental data in terms of the energy spectrum of a bottomonium. The details of the fitting procedures are explained in Appendix B.

Using the parameters m_b and α_s that were obtained, we calculate the ground state energies of a $b\bar{b}g$ through the auxiliary field method.

	σ GeV ²	α_s	m_b GeV	J^{PC}	gluon	μ_b GeV	μ_g GeV	GS energy GeV
set A	0.16	0.55	5.00	1^{--}	M	5.06	1.27	11.2
	0.16	0.55	5.00	1^{--}	E	5.17	1.10	10.6
set B	0.16	0.45	4.85	1^{--}	M	4.90	1.14	11.1
	0.16	0.45	4.85	1^{--}	E	4.98	0.94	10.6

Table III. The ground state energies of a bottomonium hybrid, and its relevant parameters. For the column of gluon, M stands for magnetic, and E means electric.

The basic inputs and outputs are summarised in Table III. From the table, it is apparent that the calculated total energies of a bottomonium hybrid are about 10.6 and 11.2 GeV for the electric gluon case and magnetic, respectively. These results are consistent with those of the QCD sum rule analyses [17].

Also, the effective mass of the constituent quark of a $b\bar{b}g$ is in the range of 4.9 to 5.1 GeV, much heavier than that (~ 1.6 GeV) of a $c\bar{c}g$. In contrast, the constituent gluon of a hybrid bottomonium is comparable to that of a hybrid charmonium in terms of effective mass: μ_g is in the range of 0.9 to 1.3 GeV, and μ_b in the range of 0.7 to 1.0 GeV for a $c\bar{c}g$.

Using these expectation values of the auxiliary fields μ_b and μ_g , we calculated the energy spectra of a bottomonium hybrid. The calculated energy spectra of a $b\bar{b}g$ are shown in the right part of Figure 6, where we can see that our theoretical values are deviated from the mass of $\Upsilon(10860)$ for both the magnetic and electric cases. In

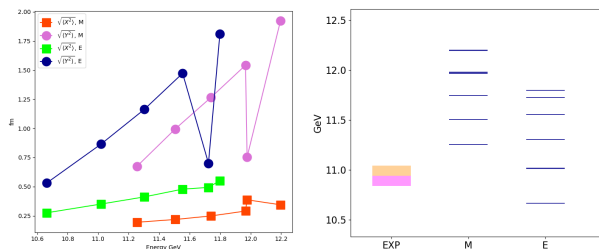


Figure 6. In the left graph, the RMS radii of X and Y are plotted against the eigen-energies for both magnetic and electric gluon cases. In the right graph, the theoretical energy spectra of a $b\bar{b}g$ are shown, where M and E means a magnetic gluon and electric, respectively. The experimental data about the spectra (of $\Upsilon(10860)$ and $\Upsilon(11020)$) are shown together [34].

the left part of Figure 6, we plot the RMS radii of X and

Y against the eigen-energies. From the graph, we can see that basically these RMS radii for the electric case are larger than those for the magnetic, which is consistent with the fact that the calculated eigen-energies of a bottomonium hybrid for the magnetic case is larger than those for the electric.

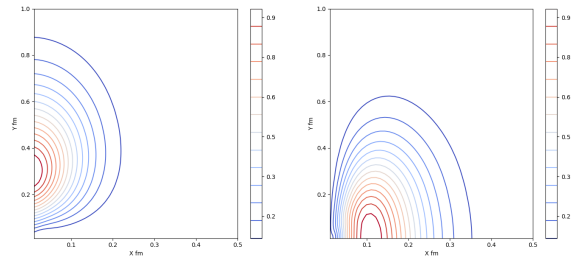


Figure 7. The probability densities of a $b\bar{b}g$ for its ground states. The left is for magnetic gluon, and the right for electric gluon. The density distributions are scaled so that their tops are unity and their bottoms are zero.

The probability densities of a bottomonium hybrid for its ground states are shown in Figure 7, where we can see the similar spatial configurations to those of a $c\bar{c}g$. This reflects the fact that $L_g = 1$ and the orbital angular momentum between b and \bar{b} is zero for the magnetic case, and that $L_g = 0$ and the orbital angular momentum between b and \bar{b} is one for the electric.

Also, we show the quark-antiquark effective potentials for the first three states of a bottomonium hybrid in Figure 8, where both the magnetic and the electric cases are considered, and the lattice calculations ($\Sigma^{+,ex}, \Pi_g$) are shown together [21]. (For the details of this Greek letter notation and the related sub- or super-scripts, see [21].) Here we show the effective potentials only for set A as they are not qualitatively different from those for set B. The calculated potentials are plotted as a function of a dimensionless quantity X/R_0 . Here R_0 is the hadronic scale parameter which is defined by $r^2 \frac{dV_{q\bar{q}}(\mathbf{r})}{dr} \Big|_{r=R_0} = 1.65$, where $V_{q\bar{q}}$ is the static quark potential [35]. The value of the parameter is about 0.5 fm [35]; in the present case, we set the parameter 0.4933 fm. We also note that the vertical axis in those graphs is made dimensionless: $R_0(V_{\text{eff}}(X) - V_{q\bar{q}}(2R_0))$.

We estimate that, for the magnetic cases, the our calculations' numerically reliable regions are $X/R_0 \in [0.4, 0.8]$ for the first two states, and $[0.5, 0.8]$ for the second excites state. For the electric cases, we estimate, the reliable regions are $X/R_0 \in [0.4, 1.4]$. The calculated potentials are smaller than those of the lattice calculations, especially for the electric cases.

C. Partial decay widths

Now we calculate the decay widths with regard to the processes of a $c\bar{c}g$ (whose constituent gluon is electric)

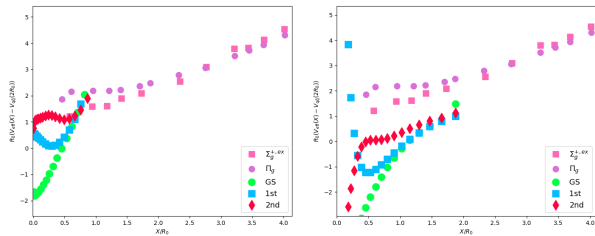


Figure 8. The calculated quark-antiquark effective potentials (set A) for the first three states of a $b\bar{b}g$. The left graph is for the magnetic gluon case and the right is for the electric. The lattice calculations ($\Sigma^{+,ex}$, Π_g) are shown together [21].

into $D^{(*)}\bar{D}^{(*)}$. Before doing this, we set relevant parameters which are given in Table IV, where ω is the averaged energy difference between the ground state and the first excited state. μ_D and μ_B are the reduced masses which are defined by

$$\mu_D = \frac{m_c m_{\bar{q}}}{m_c + m_{\bar{q}}}, \quad \mu_B = \frac{m_b m_{\bar{q}}}{m_b + m_{\bar{q}}}. \quad (25)$$

Also, introducing a Gaussian-related parameter R , we have the following relation [33]:

$$R^2 = \frac{1}{\omega\mu}. \quad (26)$$

Then, we summarise these parameters in Table IV.

	m_c or m_b GeV	ω GeV	μ_D or μ_B GeV	R GeV $^{-1}$
D meson	1.48	0.468	0.283 (0.373)	2.74 (2.39)
B meson set A	5.00	0.446	0.327 (0.454)	2.61 (2.22)
set B	4.85	0.446	0.326 (0.453)	2.62 (2.22)

Table IV. The relevant parameters for decay processes of a hybrid mesons into non-exotic mesons. Here m_c and m_b are the masses of a charm quark and bottom, respectively. The parentheses of the table stand for the values for the cases where a strange quark involves.

In this case, we set $m_q = m_{\bar{q}} = 0.35$ GeV, where $q = u, d$, and $m_s = 0.5$ GeV [33, 36]. We show the results in Table V, where we consider the decays into $D^0\bar{D}^0$, D^+D^- , $D_s^+D_s^-$, $D^{*0}\bar{D}^0$, and $D^{*0}\bar{D}^{*0}$. From the table, we see that the widths of the decays from the ground state to $D\bar{D}$ are in the range of 0.02 to 0.30 GeV, and that the total of those widths is about 0.74 GeV, much larger than the experimental data (~ 0.05 GeV) [34].

This result suggests that if the exotic meson candidate is a charmonium hybrid, it is unlikely that the $c\bar{c}g$'s constituent gluon is electric. Therefore, $\Upsilon(4260)$ contains a magnetic gluon if it is a hybrid charmonium, which is in line with earlier research [11].

As to the decays from the first excited state of a $c\bar{c}g$ to $D^{(*)}\bar{D}^{(*)}$, the sum of the partial widths is larger than

0.19 GeV. Although this value is smaller than that for the decay from the ground state, it is still much larger than the observed total widths (~ 0.1 GeV, ~ 0.06 , ~ 0.07 GeV) of $\Upsilon(4360)$, $\psi(4415)$ and $X(4660)$, respectively. This result supports the view that these exotic meson candidates are not electric-gluon hybrid mesons.

	$D^0\bar{D}^0$	D^+D^-	$D_s^+D_s^-$	$D^{*0}\bar{D}^0$	$D^{*0}\bar{D}^{*0}$	Total
$\Gamma_{GS \rightarrow D\bar{D}}$	276.21	272.71	60.04	101.19	25.90	736.0
$\Gamma_{1st \rightarrow D\bar{D}}$	64.80	63.68	29.58	23.85	14.35	196.2

Table V. The calculated widths (MeV) regarding the decays of a charmonium hybrid into $D^{(*)}\bar{D}^{(*)}$. Here the hybrid meson's constituent gluon is electric.

Next we consider the decays of a $b\bar{b}g$ into $B^0\bar{B}^0$, B^+B^- , $B^*\bar{B}^*$, $B_s\bar{B}_s$, $B_s\bar{B}_s^*$ and $B_s^*\bar{B}_s^*$. The calculated decay widths are presented in Table VI, where the experimental data are shown together [34].

As to the decay of a bottomonium hybrid which is in the ground state into $B^{(*)}\bar{B}^{(*)}$, it is apparent from the table that, for set A, the sum of the partial widths is much larger than $\Upsilon(10860)$'s total decay width (~ 51 MeV). Although, for the set B's ground state, the sum of the partial widths is comparable to $\Upsilon(10860)$'s total width, the set of parameters does not allow a $b\bar{b}g$ to decay into the states that involve B^* or B_s . For the decay into $B^0\bar{B}^0$ or B^+B^- , there are significant differences between the calculated values and the experimental data.

When it comes to the first excited state into $B^{(*)}\bar{B}^{(*)}$, for both set A and B, the sums of the partial widths are comparable to $\Upsilon(10860)$'s total width. However, our partial widths are in the order of 10^3 times greater than the experimental data in terms of the decays into $B_s\bar{B}_s$; the calculated widths are approximately 10^{-2} of the measured width for the $B_s^*\bar{B}_s^*$ channel. On top of that, the calculated $B^0\bar{B}^0$ and B^+B^- partial widths are much greater than the calculated $B^*\bar{B}^*$ partial widths, while we see the opposite in the experimental data.

Our results suggest that it seems unlikely that $\Upsilon(10860)$ is the ground state of an electric-gluon hybrid bottomonium, and that the argument that $\Upsilon(10860)$ is the first excited state of an electric-gluon $b\bar{b}g$ is weak. Having said that, we do not rule out the possibility that the first excited state of a bottomonium hybrid will be discovered as a state which is different from $\Upsilon(10860)$ since the sum of the partial widths (for set A) is around 35 MeV.

The parameter setting with regard to α_s is a matter of debate because the α_s used in (23) is identical to that used in (4). If we take the difference in energy scale into consideration, the deviations from the experimental data become smaller.

		$B^0\bar{B}^0$	B^+B^-	$B^*\bar{B}$	$B^*\bar{B}^*$	$B_s\bar{B}_s$	$B_s\bar{B}_s^*$	$B_s^*\bar{B}_s^*$	Total
set A	$\Gamma_{GS\rightarrow B\bar{B}}$	171.02	172.10	46.57	6.89	—	—	—	396.6
	$\Gamma_{1st\rightarrow B\bar{B}}$	12.79	12.88	3.54	1.38	4.08	0.42	0.03	35.1
set B	$\Gamma_{GS\rightarrow B\bar{B}}$	35.81	36.83	—	—	—	—	—	72.6
	$\Gamma_{1st\rightarrow B\bar{B}}$	31.69	31.84	10.94	7.02	6.96	1.04	0.07	89.6
$\Gamma_{exp}(\Upsilon(10860))$		2.80 ± 0.51	3.49 ± 0.81	19.43 ± 1.73	$(2.5\pm 0.2)\times 10^{-3}$	0.34 ± 0.16	8.97 ± 1.37		

Table VI. The decay widths (MeV) regarding the processes of $b\bar{b}g \rightarrow B^{(*)}\bar{B}^{(*)}$ are shown, where the experimental data about the decay of $\Upsilon(10860)$ into $B^{(*)}\bar{B}^{(*)}$ are shown together [34]. Here the hybrid meson's constituent gluon is electric.

IV. SUMMARY

In this work, we considered the possibility that $Y(4260)$, $Y(4360)$, $\psi(4415)$ or $X(4660)$ is the ground state or the first excited state of a hybrid charmonium, and also examined whether $\Upsilon(10860)$ is the ground state or the first excited state of a hybrid bottomonium.

For an electric-gluon charmonium hybrid, the calculated energy spectrum showed that the ground state appeared a few hundred MeV below the mass of $Y(4260)$, while the energy of first excited state was comparable to that of $\psi(4415)$. Also, the calculated widths for the decays of the ground state or the first excited state of a $c\bar{c}g$ into $D^{(*)}\bar{D}^{(*)}$ were much larger than the total widths of these exotic meson candidates. For a magnetic-gluon $c\bar{c}g$, the calculated ground state energy was comparable to the energy of the first excited state of an electric-gluon $c\bar{c}g$, only confirming that the calculated ground state was consistent with the results of earlier studies. Our results supported the view that if one of these exotic meson candidates is a hybrid charmonium, its constituent gluon is magnetic.

In relation to a $c\bar{c}g$, similar conclusions could be reached regarding a bottomonium hybrid. The ground states of an electric-gluon $b\bar{b}g$ appeared about two hundred MeV below the mass of $\Upsilon(10860)$, while the first

excited state was a few hundred MeV above the mass.

In addition, we evaluated the widths of the decays of the ground states and the first excited states of a $b\bar{b}g$ into $B^{(*)}\bar{B}^{(*)}$. We found that, for the ground states, some of the $B^{(*)}\bar{B}^{(*)}$ channels could not appear in our calculations, and that the widths were large to the extent that it seems unlikely that $\Upsilon(10860)$ is the ground state of an electric gluon $b\bar{b}g$. Still, there could be a possibility that the first excited state is the hybrid meson candidate, given the fact that α_s used for the calculations of the decay widths could be smaller under more realistic conditions.

When it comes to the magnetic gluon, our calculations of the ground states of a $b\bar{b}g$ are above the lattice calculations, but were in good agreement with the QCD sum rule analysis. This could be another indirect evidence to suggest that the gluonic excitations could appear in a bottomonium.

ACKNOWLEDGEMENTS

The authors thank Prof. M. Oka for many useful comments and discussions. S.Y. is supported by the Grant-in-Aid for Scientific Research (Grant No. 25247036, No. 15K17641 and No. 17K05435) from Japan Society for the Promotion of Science (JSPS), and by MEXT-Supported Program for the Strategic Foundation at Private Universities, "Topological Science" under Grant No. S1511006.

-
- | | |
|--|---|
| <p>[1] S.-K. Choi et al. Phys. Rev. Lett. 91, 262001 (2003).
 [2] M. R. Shepherd et al. Nature, 534, 487 (2016).
 [3] B. Aubert et al. Phys. Rev. Lett. 95 142001 (2005).
 [4] T. E. Coan et al. Phys. Rev. Lett. 96, 162003 (2006).
 [5] C. Z. Yuan et al. Phys. Rev. Lett. 99, 182004 (2007).
 [6] Q. He et al. Phys. Rev. D 74, 091104 (2006).
 [7] F. E. Close and P. R. Page, Phys. Lett. B 628 (2005) 215-222.
 [8] Z. Q. Liu et al. Phys. Rev. Lett. 110, 252002 (2013).
 [9] Q. Wang et al. Phys. Rev. Lett. 111 132003 (2013).</p> | <p>[10] S. Dubynskiy and M. B. Voloshin, Phys. Lett. B 666 (2008) 344.
 [11] E. Kou and O. Pene, Phys. Lett. B 631 (2005) 164-169.
 [12] A. Le Yaouanc et al, Z. Phys. C Particle and Fields 28, 309 (1985).
 [13] C. A. Meyer and E. S. Swanson, Prog. Part. Phys. 82 (2015) 21.
 [14] T. Manke et al. Phys. Rev. Lett. 82 (1999) 4396.
 [15] K. J. Juge et al, Phys. Rev. Lett. 82 (1999) 4400.
 [16] R. Berg et al. Phys. Rev. D 86, 034002 (2012).</p> |
|--|---|

- [17] C. F. Qiao et al. J. Phys. G: Nucl. Part. Phys. **39** (2012) 015005 (9p).
- [18] D. Harnett et al. J. Phys. G: Nucl. Part. Phys. **39** (2012) 125003 (11pp).
- [19] N. Brambilla et al. arXiv:1805.07713 [hep-ph].
- [20] M. Berwein et al. Phys. Rev. D **92** (2015) 114019.
- [21] K. J. Juge et al. Nucl. Phys. B (Proc. Suppl.) **63** A-C (1998) 326.
- [22] T. J. Allen et al. Phys. Lett. B **434** (1998) 110.
- [23] M. Lüscher and P. Weisz, JHEP07 (2002) 049.
- [24] R. Oncala and J. Soto, Phys. Rev. D **96** 014004 (2017).
- [25] Yu. S. Kalashnikova and A. V. Nefediev, Phys. Rev. D **77** 054025 (2008).
- [26] V. Mathieu, Phys. Rev. D **80**, 014016 (2009).
- [27] K. Becker, M. Becker and J. H. Schwarz. String Theory and M-Theory: A Modern Introduction, Cambridge University Press (2007).
- [28] Yu. S. Kalashnikova and A. V. Nefediev, Phys. At. Nucl. **68** (2005) 650.
- [29] Yu. S. Kalashnikova et al. Phys. Rev. D **64**, 014037 (2001).
- [30] W. Zickendraht, Ann. of Phys. **35**, 18 (1965).
- [31] J. L. Ballot and M. F. De La Ripelle, Ann. Phys. **127** 62-125 (1980).
- [32] F. Buisseret and C. Semay, Phys. Rev. D **74**, 114018 (2006).
- [33] F. Iddir et al. Phys. Lett. B **433** (1998) 125-138.
- [34] C. Patrignani et al. (Particle Data Group), Chin. Phys. C, **40**, 100001 (2016).
- [35] C. J. Morningstar and M. Peardon, Phys. Rev. D **56**, 4043 (1997).
- [36] F. Iddir and A. S. Safir, Phys. Lett. B **507** (2001) 183.
- [37] M. Tanabashi et al. (Particle Data Group), Phys. Rev. D **98**, 030001 (2018).
- [38] J. Raynal and J. Revai, Nuovo Cimento, A **68**, 612 (1970).
- [39] J. Raynal, Nucl. Phys. A **202** (1973) 631.
- [40] R. I. Jibuti et al. Nucl. Phys. A **276** (1977) 421.
- [41] T. Yoshida et al. Phys. Rev. D **92** 114029 (2015).
- [42] D. Baye, Phys. Rep. **565** (2015) 1-107.
- [43] C. Semay et al, Phys. Rev. E **64**, 016703-1 (2001).
- [44] F. Buisseret and C. Semay, Phys. Rev. E **75** 026705 (2007).

Appendix A: The coordinate systems of a three-body system

This section covers the hyperspherical and the Jacobi coordinates for a three-body system which consists of particle 1, 2 and 3; their masses are denoted by m_1, m_2 and m_3 , respectively.

For the present case, there exist three different types of the Jacobi coordinates: X-coordinates, Y-coordinates and T-coordinates (See Figure 9). In the figure, X_1 is the distance between particle 1 and 3, and Y_1 is the distance between particle 2 and the centre-of-mass of particle 1 and 3. Similar things hold true for X_2, Y_2 and X_3, Y_3 . Picking up one of these coordinates, we can express the

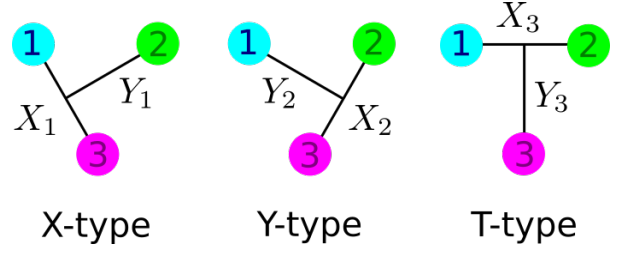


Figure 9. The three different types of the Jacobi coordinates.

Jacobi coordinates by [39]:

$$\mathbf{x}_i = \sqrt{\frac{m_j m_k}{m_j + m_k}} (\mathbf{r}_j - \mathbf{r}_k), \quad (\text{A1})$$

$$\mathbf{y}_i = \sqrt{\frac{m_i (m_j + m_k)}{M}} \left(\mathbf{r}_i - \frac{m_j \mathbf{r}_j + m_k \mathbf{r}_k}{m_j + m_k} \right), \quad (\text{A2})$$

$$\mathbf{R} = \frac{m_1 \mathbf{r}_1 + m_2 \mathbf{r}_2 + m_3 \mathbf{r}_3}{M}, \quad (\text{A3})$$

where $M = m_j + m_k + m_i$, and (i, j, k) is a cyclic permutation of $(1, 2, 3)$. Then, we note that the three different Jacobi coordinates (X, Y and T) are connected to each other via the kinematic rotation:

$$\begin{pmatrix} \mathbf{x}_k \\ \mathbf{y}_k \end{pmatrix} = \begin{pmatrix} -\cos \phi_{ki} & \sin \phi_{ki} \\ -\sin \phi_{ki} & -\cos \phi_{ki} \end{pmatrix} \begin{pmatrix} \mathbf{x}_i \\ \mathbf{y}_i \end{pmatrix}, \quad (\text{A4})$$

where ϕ_{ki} is the angle of the kinematic rotation. Specifically, the angle is $\phi_{ki} = \arctan(-1)^P \sqrt{\frac{M m_j}{m_i m_k}}$, where P is determined according to the permutation of (123). P is even/odd when (kij) is an even/odd permutation of (123).

When it comes to a hyperspherical coordinate system, we introduce a quantity which does not depend on the three coordinates (X, Y and T) by the following identities:

$$x_1^2 + y_1^2 = x_2^2 + y_2^2 = x_3^2 + y_3^2 = \rho^2, \quad (\text{A5})$$

where the hyperradius ρ has already been defined in (9). We note that from the definition of the kinematic rotation, it is apparent that $\{x_i^2 + y_i^2\}_{i=1,2,3}$ are invariant quantities under the rotation. Then, x_i and y_i are expressed as [38]:

$$x_i = \rho \cos \alpha_i, \quad y_i = \rho \sin \alpha_i, \quad (\text{A6})$$

where $\{\alpha_i\}_{i=1,2,3}$ are hyperangles. By using the ρ and α_i , we can define the hyperspherical harmonics (11). Accordingly, it is possible that we express the hyperspherical harmonics in three different ways: $\{\mathcal{Y}_{KLM}^{L_{x_i}, L_{y_i}}(\Omega_{5,i})\}_{i=1,2,3}$. These different HHs are linked to each other via the Raynal-Revai coefficients: $\langle L_{x_k} L_{y_k} | L_{x_i} L_{y_i} \rangle_{KL}$ [38].

In addition to the coordinates \mathbf{x}, \mathbf{y} and \mathbf{R} , we need to mention their conjugate momenta $\boldsymbol{\kappa}_x, \boldsymbol{\kappa}_y, \mathbf{P}$. They are

given by [40]:

$$\boldsymbol{\kappa}_x = \sqrt{\frac{m_j m_k}{m_j + m_k}} \left(\frac{\mathbf{k}_j}{m_j} - \frac{\mathbf{k}_k}{m_k} \right), \quad (\text{A7})$$

$$\boldsymbol{\kappa}_y = \sqrt{\frac{m_i(m_j + m_k)}{M}} \left(\frac{\mathbf{k}_j + \mathbf{k}_k}{m_j + m_k} - \frac{\mathbf{k}_i}{m_i} \right) (-1), \quad (\text{A8})$$

$$\mathbf{P} = \sqrt{\frac{1}{M}} (\mathbf{k}_1 + \mathbf{k}_2 + \mathbf{k}_3). \quad (\text{A9})$$

The factor (-1) for $\boldsymbol{\kappa}_y$ does not exist in Jibuti's paper; this factor is just a matter of choice. Here, $\boldsymbol{\kappa}$ is defined by $\boldsymbol{\kappa}^2 = \boldsymbol{\kappa}_x^2 + \boldsymbol{\kappa}_y^2$ [40]. Relating to the hyperspherical coordinates, we have $\kappa_x = \kappa \cos \alpha_\kappa$ and $\kappa_y = \kappa \sin \alpha_\kappa$.

Appendix B: Fitting procedures

In this section, we show the basic fitting procedures with regard to the relevant parameters of a bottomonium. We determine the values of the string tension σ and the colour-Coulomb parameter α_s by fitting them to the energy spectrum of a $b\bar{b}$. Firstly we need to set the Hamiltonian $H_{\text{tot}}^{b\bar{b}}$ for the two-body system:

$$H_{\text{tot}}^{b\bar{b}} = H_0^{b\bar{b}} + V_{\text{Lin+Cou}}^{b\bar{b}} + V_{\text{str}}^{b\bar{b}} + V_{\text{LS}}^{b\bar{b}} + V_{\text{ss}}^{b\bar{b}} + V_{\text{ST}}^{b\bar{b}}, \quad (\text{B1})$$

where $H_0^{b\bar{b}}$ is the free Hamiltonian for the bottomonium; $V_{\text{Lin+Cou}}^{b\bar{b}}$ is the term of the linear and colour-Coulomb potentials; $V_{\text{str}}^{b\bar{b}}$ is a string correction term. In addition, we use the LS coupling term $V_{\text{LS}}^{b\bar{b}}$, the spin-spin interaction $V_{\text{ss}}^{b\bar{b}}$ and the tensor term $V_{\text{ST}}^{b\bar{b}}$. These interactions are explicitly shown as follows:

$$\begin{aligned} V_{\text{str}}^{b\bar{b}} &= -\frac{\sigma \mathbf{L}^2}{6\mu^2 r} (\hbar c) \\ V_{\text{LS}}^{b\bar{b}} &= -\frac{\sigma}{2\mu^2 r} (\mathbf{L} \cdot \mathbf{S}) (\hbar c) + \frac{2\alpha_s}{\mu^2 r^3} (\mathbf{L} \cdot \mathbf{S}) (\hbar c)^3 \\ V_{\text{ss}}^{b\bar{b}} &= \frac{32\pi\alpha_s}{9\mu^2} (\mathbf{s}_q \cdot \mathbf{s}_{\bar{q}}) \delta(\mathbf{r}) (\hbar c)^3 \\ V_{\text{ST}}^{b\bar{b}} &= \frac{4\alpha_s}{3\mu^2 r^5} [3(\mathbf{s}_q \cdot \mathbf{r})(\mathbf{s}_{\bar{q}} \cdot \mathbf{r}) - r^2(\mathbf{s}_q \cdot \mathbf{s}_{\bar{q}})] (\hbar c)^3, \end{aligned}$$

where we explicitly write $\hbar c$ factors as well. We replace the delta function which appears in the spin-spin interaction with the following exponential function [41]:

$$\delta(\mathbf{r}) \rightarrow \frac{\Lambda^2}{4\pi r} e^{-\Lambda r}. \quad (\text{B2})$$

We make this sort of modification in part because we cannot treat the delta function numerically; also we need to address numerical instability issues relating to the delta function. Also, we modify the tensor interaction as follows [41]:

$$V_{\text{ST}}^{b\bar{b}} \rightarrow \frac{\alpha_s (1 - e^{-\Lambda r})^2}{3\mu^2 r^3} S_{12} (\hbar c)^3, \quad (\text{B3})$$

where $S_{12} = 12(\mathbf{s}_b \cdot \mathbf{n})(\mathbf{s}_{\bar{b}} \cdot \mathbf{n}) - 4(\mathbf{s}_b \cdot \mathbf{s}_{\bar{b}})$.

	set A	set B	E_{exp}
	GeV	GeV	GeV
$\chi_{b2}(1P)$	3P_2	10.176 9.964	$9.91221 \pm (0.57 \times 10^{-3})$
$h_b(1P)$	1P_1	10.147 9.945	$9.8993 \pm (0.8 \times 10^{-3})$
$\chi_{b1}(1P)$	3P_1	10.093 9.927	$9.89278 \pm (0.57 \times 10^{-3})$
$\chi_{b0}(1P)$	3P_0	10.014 9.893	$9.85944 \pm (0.73 \times 10^{-3})$
$\Upsilon(1S)$	3S_1	9.426 9.401	$9.46030 \pm (2.6 \times 10^{-4})$
$\eta_b(1S)$	1S_0	9.395 9.381	$9.3990 \pm (2.3 \times 10^{-3})$

Table VII. The calculated energy spectra, and the measured one with regard to a bottomonium. The parameters are $m_b = 5.00$ GeV and $\alpha_s = 0.55$ for set A, and $m_b = 4.85$ and $\alpha_s = 0.45$ for set B. $\Lambda = 6.0$ (1/fm). The experimental data are from [34].

Secondly, we changed the mass m_b of a bottom quark, and calculated the energy spectrum, fixing σ and α_s . We used the auxiliary field method to determine the ground state and the value of a relevant auxiliary field. After obtaining these values, we calculated the higher states of a charmonium.

The results are shown in the set A column of Table VII, where we can see that the calculated energies agree with the experimental data for the bottom two states. When it comes to higher states, the difference between our values and the experimental data is more than 1.5 per cent.

Then, we changed both m_b and α_s and searched the parametrisation under which the calculated energy well reproduces the $b\bar{b}$ energy spectrum. Accordingly we get $\alpha_s = 0.45$ and the corresponding energy spectrum which is shown in the set B column of Table VII. This parametrisation produces the theoretical values that are consistent with the experimental results.

Finally, we present the summary of the parameter sets in Table VIII.

	σ	α_s	Λ	m_b	μ
	GeV ²		fm ⁻¹	GeV	GeV
set A	0.16	0.55	6.0	5.00	5.42
set B	0.16	0.45	6.0	4.85	5.16

Table VIII. The relevant parameter sets for a bottomonium.

Appendix C: Lagrange mesh technique

In this section, we explain the Lagrange mesh method.

Suppose the Lagrange functions $\{f_j\}_{j=1,\dots,N}$ are real functions, and $\{z_j\}_{j=1,\dots,N}$ are their mesh points; the set of these points is the quadrature-point-equivalent in the

Gauss quadrature. Then, the Lagrange functions satisfy the following condition [42]:

$$f_i(z_j) = \frac{\delta_{ij}}{\sqrt{\lambda_i}}. \quad (\text{C1})$$

We can easily check that the functions are orthonormal:

$$\langle f_i | f_j \rangle_G = \sum_{k=1}^N \lambda_k \frac{\delta_{ik}}{\sqrt{\lambda_i}} \frac{\delta_{jk}}{\sqrt{\lambda_j}} = \lambda_i \frac{\delta_{ji}}{\sqrt{\lambda_i \lambda_j}} \quad (\text{C2})$$

$$= \delta_{ij}, \quad (\text{C3})$$

where the brackets $\langle \cdot | \cdot \rangle_G$ stands for the Gauss quadrature calculation.

1. Scaling

In actual calculations, it is convenient to introduce scaling to reduce the computational cost. Here we denote the scaling parameter by x_0 such that $z = \frac{x}{x_0}$.

Suppose the T-operator is $T = -\frac{d^2}{dx^2}$. Then, using the scaled parameter z and the scaled Lagrange functions $\{f(x/x_0)\}_{j=1, \dots, N}$, we can write it matrix element as:

$$\int f_i^*(x/x_0) T f_j(x/x_0) dx = x_0 \int f_i^*(z) \left(-\frac{d}{d(x_0 z)^2} \right) f_j(z) dz = x_0 T_{ij}, \quad (\text{C4})$$

where the matrix element T_{ij} contains the scaling parameter:

$$T_{ij} = \frac{1}{x_0^2} \int f_i^*(z) \left(-\frac{d}{dz^2} \right) f_j(z) dz. \quad (\text{C5})$$

We also calculate the matrix element of a potential $V(x)$ by this scaled functions:

$$\int f_i^*(x/x_0) V(x) f_j(x/x_0) dx = x_0 V(x_0 z_i) \delta_{ij}. \quad (\text{C6})$$

When it comes to the wave function, we expand it so as to keep the normalisation

$$\psi(x) = \frac{1}{\sqrt{x_0}} \sum_{j=1}^N c_j f_j(x/x_0). \quad (\text{C7})$$

It follows from these expressions that the equations of motion are written as

$$\sum_{j=1}^N (T_{ij} + V(x_0 z_i) \delta_{ij} - E \delta_{ij}) c_j = 0, \quad (\text{C8})$$

where, for simplicity, the (reduce) mass parameter μ and the reduced Planck constant \hbar are set unity.

Also we note that in practice, the Gauss quadrature does not yield accurate matrix elements for Coulomb-type and centrifugal-type potentials [42]; in addition, we often use non-orthogonal Lagrange functions. For these reasons, we use the regularised functions which are given by

$$\tilde{f}_j(z) = \frac{z}{z_j} f_j(z) = (-1)^j \sqrt{\frac{1}{z_j h_n^{(\alpha)}}} z^{1+\frac{\alpha}{2}} e^{-\frac{z}{z_j}} \frac{L_n^{(\alpha)}(z)}{z - z_j}. \quad (\text{C9})$$

This expression allows us to realise that the regularised functions still satisfy the condition (C1): $\tilde{f}_j(z_k) = \frac{z_k}{z_j} f_j(z_k)$. The shortcoming of the regularised functions is that they do not form an orthonormal set:

$$\langle \tilde{f}_i | \tilde{f}_j \rangle = \delta_{ij} + \frac{(-1)^{i-j}}{\sqrt{z_i z_j}}, \quad (\text{C10})$$

where the brackets $\langle \cdot | \cdot \rangle$ means the norm or matrix element calculation where no approximation is used. It could be noteworthy that we could treat the basis function like orthonormal functions because numerical experiments suggest that ignoring the non-orthogonality does not lead to a significant loss of accuracy [42].

The matrix elements of the double differential operator is expressed as:

$$T_{ij} = \frac{1}{x_0^2} t_{ij} \quad (\text{C11})$$

$$t_{ij} = \begin{cases} \frac{(-1)^{i-j+1}}{4\sqrt{z_i z_j}} + (-1)^{i-j} \frac{z_i + z_j}{\sqrt{z_i z_j} (z_i - z_j)^2} & \text{for } i \neq j \\ \frac{(-1)^{i-j+1}}{4\sqrt{z_i z_j}} - \frac{z_i^2 - 2(2N + \alpha + 1)z_i + (\alpha^2 - 4)}{12z_i^2} & \text{for } i = j \end{cases}. \quad (\text{C12})$$

2. Salpeter-type Hamiltonian

We can use the Lagrange mesh technique to solve the eigenvalues problems which involves the Salpeter

Hamiltonian: $H = \sqrt{\mathbf{p}^2 + m^2} + V$. The procedure to calculate the matrix elements of $\sqrt{\mathbf{p}^2 + m^2}$ is shown as

follows [43]:

1. Calculate $P_{ij}^2 = \langle \tilde{f}_i | \mathbf{p}^2 + m^2 | \tilde{f}_j \rangle$
2. Diagonalise $P_{ij}^2 = VD^2V^{-1}$
3. Derive D by calculating the positive square root of each element of D^2
4. Obtain the matrix elements through $P_{ij} = VDV^{-1}$

3. Solving inverse problems

After obtaining the wave function and the eigen-energy of a system, we use (C1) and (C7) to obtain the relation between the expansion coefficients and the wave function:

$$c_k = \sqrt{x_0 \lambda_k} \phi(x_k) . \quad (\text{C13})$$

This relation allows us to solve the inverse problem where the eigen-energy and the wave function are used as inputs. We substitute this relation into (C8) to have the expression for the potential [44]. (We note that here the reduce Planck constant is set unity.):

$$V(x_i) = E - \sum_{j=1}^N T_{ij} \frac{\sqrt{\lambda_j} \phi(x_j)}{\sqrt{\lambda_i} \phi(x_i)} . \quad (\text{C14})$$

Appendix D: Momentum representation

In this short section, we briefly show the momentum representation of the wave function for a hybrid meson. This is used for the calculations of widths for the processes of $c\bar{c}g \rightarrow D^* \bar{D}^*$, and $b\bar{b}g \rightarrow B^* \bar{B}^*$. In relation to this, it is worth mentioning that the whole wave function of a quarkonium hybrid, which is originally expressed in the hyperspherical coordinates, is rewritten by using the Cartesian coordinates:

$$\Psi(\mathbf{X}, \mathbf{Y}) = \sum_{S_{tot}} R(X, Y) [[Y_{L_{q\bar{q}}} \otimes Y_{L_g}]_{L_{tot}} \otimes [|S_{q\bar{q}}\rangle \otimes |S_g\rangle]_{S_{tot}}]_{JM_J} , \quad (\text{D1})$$

where the relating subscripts are omitted in $R(X, Y)$ for simplicity.

After that, we use the Rayleigh expansion to conduct Fourier transformation:

$$\begin{aligned} e^{i(\mathbf{K}_1 \cdot \mathbf{r}_1 + \mathbf{K}_2 \cdot \mathbf{r}_2)} &= (2\pi)^3 \sum_{L_1, L_2, m_1, m_2} i^{L_1} i^{L_2} \frac{1}{\sqrt{K_1 r_1}} \cdot \frac{1}{\sqrt{K_2 r_2}} \\ &\times J_{L_1+1/2}(K_1 r_1) J_{L_2+1/2}(K_2 r_2) \\ &\times Y_{L_1 m_1}^*(\hat{\mathbf{K}}_1) Y_{L_1 m_1}(\mathbf{r}_1) Y_{L_2 m_2}^*(\hat{\mathbf{K}}_2) Y_{L_2 m_2}(\mathbf{r}_2) . \end{aligned} \quad (\text{D2})$$

Then, we obtain the expression for the momentum representation Φ_{JM_J} of the whole wave function:

$$\Phi_{JM_J}(\mathbf{p}_{q\bar{q}}, \mathbf{k}_g) = \sum_{S_{tot}} (2\pi)^3 \tilde{R}(p_{q\bar{q}}, k_g) [[Y_{L_{q\bar{q}}} \otimes Y_{L_g}]_{L_{tot}} \otimes [|S_{q\bar{q}}\rangle \otimes |S_g\rangle]_{S_{tot}}]_{JM_J} \quad (\text{D3})$$

$$\begin{aligned} &= \sum_{S_{tot}} (2\pi)^3 \tilde{R}(p_{q\bar{q}}, k_g) \sum_{J_{q\bar{q}}, J_g} X(L_{q\bar{q}} L_g L_{tot}, S_{q\bar{q}} S_g S_{tot}, J_{q\bar{q}} J_g J) \\ &\times [[Y_{L_{q\bar{q}}} \otimes |S_{q\bar{q}}\rangle]_{J_{q\bar{q}}} \otimes [Y_{L_g} \otimes |S_g\rangle]_{J_g}]_{JM_J} , \end{aligned} \quad (\text{D4})$$

where $X(abc, def, ghi)$ is defined by

$$\begin{aligned} X(abc, def, ghi) &= \sqrt{(2c+1)(2f+1)(2g+1)(2h+1)} \\ &\times \begin{Bmatrix} a & b & c \\ d & e & f \\ g & h & i \end{Bmatrix} . \end{aligned} \quad (\text{D5})$$

Finally, putting

$$\begin{aligned} \hat{\Phi}_{J_{q\bar{q}} J_g}(\mathbf{p}_{q\bar{q}}, \mathbf{k}_g) &= \sum_{S_{tot}} (2\pi)^3 \tilde{R}(p_{q\bar{q}}, k_g) \\ &\times X(L_{q\bar{q}} L_g L_{tot}, S_{q\bar{q}} S_g S_{tot}, J_{q\bar{q}} J_g J) \\ &\times [[Y_{L_{q\bar{q}}} \otimes |S_{q\bar{q}}\rangle]_{J_{q\bar{q}}} \otimes [Y_{L_g} \otimes |S_g\rangle]_{J_g}]_{JM_J} , \end{aligned} \quad (\text{D6})$$

we express $\Phi_{JM_J}(\mathbf{p}_{q\bar{q}}, \mathbf{k}_g)$ as

$$\Phi_{JM_J}(\mathbf{p}_{q\bar{q}}, \mathbf{k}_g) = \sum_{J_{q\bar{q}} J_g} \hat{\Phi}_{J_{q\bar{q}} J_g}(\mathbf{p}_{q\bar{q}}, \mathbf{k}_g) . \quad (\text{D7})$$